A THESIS

FOR THE DEGREE OF MASTER OF PHYLOSOPHY

Grid Voltage Control of Offshore DFIG-Based Wind Farm for Connecting LCC-HVDC System

Pham Van Hoan

Faculty of Applied Energy System
Major of Electrical Engineering

GRADUATE SCHOOL
JEJU NATIONAL UNIVERSITY

2010.8

Grid Voltage Control of Offshore DFIG-Based Wind Farm for Connecting LCC-HVDC System

Pham Van Hoan

(Supervised by Professor Eel Hwan Kim)

A thesis submitted in partial fulfillment of the requirement for

the degree of Master of Philosophy

2010. 08.

This thesis has been examined and approved.

Chongkeun Jwa

Thesis director, Chong-Keun Jwa, Prof. of Electrical Engineering

Se-Ho Kim, Prof. of Electrical Engineering

Eel Hwan Kim

Eel-Hwan Kim, Prof. of Electrical Engineering

MAJOR OF ELECTRICAL ENGINEERING

FACULTY OF APPLIED ENERGY SYSTEM

GRADUATE SCHOOL

JEJU NATIONAL UNIVERSITY

REPUBLIC OF KOREA

To

My Parents

Acknowledgements

I would like to express my deep appreciation and sincere gratitude to Prof. Eel Hwan Kim, my supervisor, for his wisdom, invaluable guidance and professionalism from the beginning to the end in the course of my research. His patience was extraordinary and I would like to thank him especially for that. I have learned a lot from him both as a teacher and a friend and most importantly to keep smiling all the while.

Besides my advisors, I would like to thank the rest of my thesis committee, Prof. Chong Keun Jwa, Prof. Se Ho Kim, who asked me good questions, gave insightful comments and reviewed my work on a very short notice.

I am indebted to other Professors at the Department of Electrical Engineering, Prof. Seong Bo Oh, Prof. Kae Myoung Lee and Prof. Ho Chan Kim who taught me during the Master's course. They continually and convincingly conveyed a spirit of adventure in regard to research and scholarship, and an excitement in regard to teaching. Without their guidance and persistent help this dissertation would not have been possible.

A special thanks to our group, Jae Hong Kim, Jin Hong Ahn, Dae Hyun Kim, Seung Hyun Kim, Myung Suk Kang, Yong Gi Kim for all their input during our meetings and in the lab.

The days would have passed far more slowly without the support, and advice of my true friends, Tran Thi Thanh Khuong, Quach Ngoc Thinh, Nguyen Van Quyen and Le Thanh Cuong, whom I thank for putting up with my idiosyncrasies and for providing such a rich source of conversation, education and entertainment.

Last but not least, I wish to thank my parents for their love and encouragement, without whom I would never have enjoyed so many opportunities.

Abbreviations

AC	Alternating Current
DC	Direct Current
DFIG	Doubly Fed Induction Generator
DVR	Dynamic Voltage Restorer
ESCR	Effective Short Circuit Ratio
EWEA	European Wind Energy Association
FACTS	Flexible AC Transmission System
FRT	Fault Ride Through
GTO	Gate-Turn-Off
HVAC	High Voltage Alternating Current
HVDC	High Voltage Direct Current
IGBT	Insulated Gate Bipolar Transistor
LCC	Line-Commutated Converter
OHL	Overhead Line
SCR	Short Circuit Ratio
SMES	Superconducting Magnetic Energy Storage
SSC	Static Series Compensator
STATCOM	Static Compensator
VSC	Voltage Source Converter
WPPs	Wind Power Plants
WTG	Wind Turbine Generator

Contents

List of Figures

List of Tables

요 약

오늘날 전 세계적으로 신재생에너지 중 풍력발전이 가장 상용화에 성공하여 하나의 전력에너지원으로서 크게 역할을 하고 있다. 초기에는 주로 육상풍력에 많은 투자가 이루어지고 또한 단지별 풍력발전단지의 용량은 전력계통의 안정을 위하여 접속점에서의 계통용량에 10% 이하가 되도록 하여 운영하였다.

하지만 풍력발전시스템기술이 발전과 더불어 단위 출력당 발전단가가 일반 화력발전소보다도 낮아지면서 설비용량은 크게 증가하였고 또한 단지별 용량도 크게 증가 하였다. 이러한 현상은 풍력발전 시스템을 도입하여 운용하는 대부분의 국가에서 나타나고 있다. 그러나 용량이 커지면서 불규칙한 출력변동에 따른 계통의 안정도는 점점 나빠져 이에 대한 대비책이 꾸준하게 요구되어 왔다. 특히 계통 접속점에서의 용량이 10% 가 넘는 대규모 풍력발전단지에서는 이러한 문제가 아주 중요한 계통안정도의 선결과제가 되었다. 더구나 오늘날 전 세계적으로 해상풍력발전단지 개발이 큰 화두로 되고 있는 현실에서 이 문제는 더욱 중요한 문제가 되어 왔다. 그래서 육상에서 100km 이상 떨어지고 용량이 200MW 이상인 해상풍력발전 시스템은 거의 HVDC 시스템을 통하여 육지의 계통과 연계를 하고 있다. HVDC 시스템은 전압과 전류형으로 구분되는데 전압형은 유효출력전력과 무효출력전력을 독립적으로 제어 할 수 있다는 장점과 풍력발전 출력을 손쉽게 역송할 수 있다는 장점이 있지만 전류형에 비해 가격과 전력변환시스템 손실부분에서 단점을 가진다. 반면에 전류형은 용량이 전압형에 크고 또한 시스템의 운전경험이 많아 신뢰성이 크다는 장점이 있다. 하지만 사이리스터 on-off 를 위한 무효전력이 반드시 필요하다는 단점을 가진다.

따라서 본 연구에서는 DFIG 로 구성된 해상풍력발전 용량이 500MW 이고 육지와의 연계를 전류형 HVDC 를 채용하여 운전할 때 갑작스런 계통전압 감소에 따른 풍력발전단지의 운전정지방지를 위하여 제안된 순간전압보상기를 가지고 계통전압감소에 따른 순간전압강하분 만큼 보상전압을 출력시켜 풍력발전단지가

계통전압강하에 따른 출력정지를 방지하도록 한다. 뿐만 아니라 제안한 순간전압보상기의 동특성을 확인하기 위하여 단위계단별 출력변화 입력에 대한 순간전압기의 출력 특성을 분석한다. 이와 같은 해석은 전력계통과 전력전자시스템을 해석하는데 유용한 PSCAD/EMTDC 프로그램을 이용하여 이를 수행한다. 해석한 결과를 분석해 보면 순간전압보상기와 DFIG를 채용한 풍력발전단지 그리고 전류형 HVDC 모델링이 잘되어 양호한 출력 특성을 얻을 수 있어 이를 해상풍력발전 단지에 적용시 유용하리라 사료된다.

1. Introduction

1.1 New trends of power transmission from the large wind farms

Wind turbine generators (WTG) convert wind energy into electrical energy. Now large wind turbines of up to 5MW size have been developed. A wind farm, also known as wind power plant (WPP), is a collection of a few tens or a few hundreds of WTG installed in close vicinity. They are connected to the collector bus by cables. The electric power aggregated at the collector bus has to be fed into the power grid network for transmission and distribution to the load centers and utilities located hundreds of km away.

A vast majority of generation, transmission, distribution and consumption of electric power is in the form of AC. Hence, HVAC transmission is the obvious choice for the grid connection of wind farm. Most of the operational wind farms are connected using HVAC connection. The HVAC option is the most suitable and economic where the wind farm capacity is less than 150 MW and is within 100-150 km from the main grid. Conventionally, AC connection has been used that offers some advantages such as low cost, relatively simple layout, the proven technology, etc. Yet for large wind farms with a long transmission distance, there are some serious disadvantages with AC connection technology:

• Long AC cables produce large amounts of capacitive current, which can significantly reduce the cable transmission capacity and require large reactive power compensation;

• AC connections result in synchronous operation between the wind farm and the grid; therefore, faults occurring on the grid will directly affect the wind farm and vice versa.

Presently AC cables have a maximum cable rating of about 200MW per three phase cable, on a voltage level of 150 - 170kV, compensation at both ends and maximum cable length of around 200km. For a shorter distance of a 100km, voltage ratings may be raised to 245kV, thereby increasing the power transfer capability to 350MW [1]. As shown in Fig. 1.1, HVAC

transmission is not feasible for large offshore power plants requiring cable transmission over long distances.

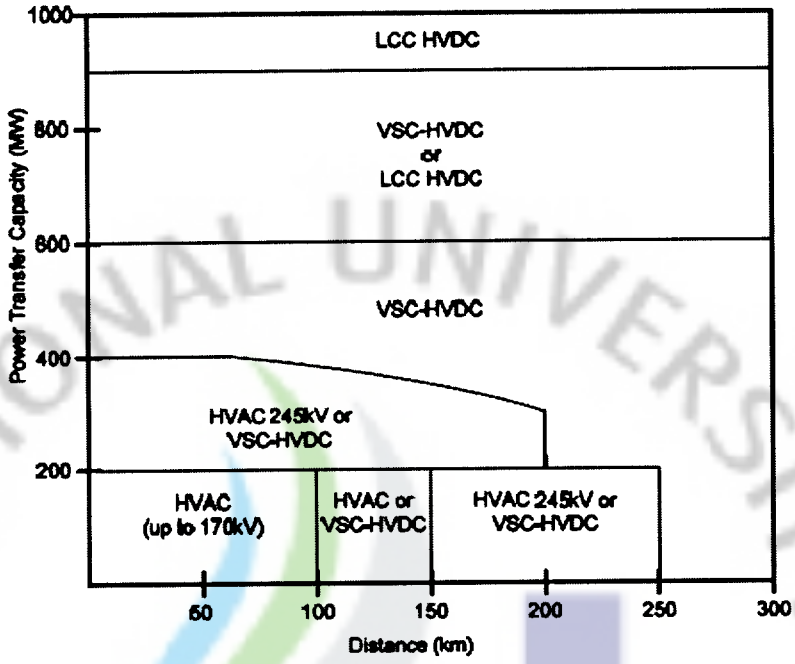

Fig. 1.1 Choice of transmission technology for different wind farm capacities and distances [1].

Unlike HVAC transmission systems, there is no reactive power generation or absorption in HVDC transmission systems. Hence, HVDC transmission is very suitable for bulk power transmission over long distances. This has been one of the driving factors for the development of HVDC systems since the first commercial installation in Gotland in the year 1954. The main advantages of HVDC over AC transmission are [2]:

- Power flow is fully controlled.
- The offshore grid voltage and frequency are decoupled from the onshore network; therefore, disturbances on one side of the HVDC system will not directly affect the other.
- Dc transmission is not affected by cable charging currents which reduce the active power transmission capacity of an AC cable as the length increases.

Two alternative technologies for the HVDC converters are available, a voltage source converter (VSC) using IGBTs, and a line-commutated converter (LCC) using thyristors.

A comparison of LCC-HVDC (referred as HVDC Classic) and VSC-based HVDC is given in Table 1.1 [3].

Table 1.1 Comparison of LCC-based HVDC and VSC-based HVDC.

		LCC-based HVDC	VSC-based HVDC
1	Size range single convertor	150 – 1500 MW	50 – 550 MW
2	Convertor/Semiconductor technology	Line commutated, Thyristor	Self commutated, IGBT
3	Relative volume	4 – 6 times	1
4	Type of cable	Mass Impregnated Paper Oil/Paper	XLPE
5	Control of active power	Yes	yes
6	Control of reactive power	No (only switched regulation)	Yes, continuous control
7	Voltage control	Limited	Extensive
8	Fault ride-through	No	Yes
9	Black start capability	No	Yes
10	Minimum short circuit capability in AC grid	>2.0 x rated power	No requirement
11	Power reversal with-out interruption	No	Yes
12	Generator needed on off-shore platform	Yes	No requirement
13	Minimum DC power flow	5-10% of rated power	No minimum DC power
14	Typical losses per convertor	0.8%	1.6%
15	Operating experience	> 20 years	8 years
16	Operating experience off-shore	No	Yes

1.2 Aims and outline of the thesis

The control paradigms of the LCC HVDC connection for a DFIG driven wind farm have been presented in previous publications [4]-[7]. During fault on the main grid, the group of solutions based on a fast reduction of the generated power in the wind park was displayed. The most popular methods to achieve this behavior are grid frequency control [4],[6],[7] and direct communication between STATCOM and generators [4]. In the first method shown in [4], a communication delay of 30ms results in a maximum voltage on the STATCOM DC side of 3 p.u. and temporary power absorption of 2.4 p.u. However, the communication delay in the worst-case is practically much higher and is about 100ms as mentioned in [8]. The method of frequency control is also shown in [4], and a lower STATCOM DC over-voltage of 1.8 p.u. and power absorption of 2 p.u. are simulation results of onshore fault lasting only

100ms. In [6] the grid frequency control is used to regulate the HVDC rectified firing angle and shows a good control performance under operational and fault condition. However, a ride through paradigm of loss-of-supply faults (or main-grid voltage sags) with practical fault detection algorithm in the DFIG controllers is not addressed. On the other hand, it seems that local load is not properly considered in the studies. Especially if the local load has synchronously rotating equipment that is sensitive to frequency deviations, the frequency can be not changed freely. Moreover, another drawback of frequency control measure is a phase-locked loop (PLL) circuit applied for measuring the frequency. A typical PLL has a first order time response, causing an inherent delay aggravating the speed of response of the frequency-dependent control loop. A typical time delay lies in the range 10-100ms. Making the PLL faster is possible, but makes the system very sensitive to measurement noise, which is the main reason that a slower PLL is preferred for practical applications.

Another method of the generated power reduction by lowering the wind park network voltage has been almost not shown in any studies in terms of LCC-HVDC link connection. This method has not received adequate attention perhaps because the commutation failure of the HVDC is very sensitive to voltage magnitude at the HVDC rectifier. This thesis uses this measure to achieve a fast power reduction, and the local load is always kept at a stable and continuous state.

When LCC HVDC system is used in power transmission, the STATCOM will be usually connected to provide the necessary commutation voltage to the HVDC. This is almost compulsory in LCC HVDC. And this connection has also demonstrated its effectiveness and necessity in power transmission [4] and [5]. In addition, another effective control method without using STATCOM was also presented in [6]. However, besides the STATCOM, in the FACTS concept, there are still other promising devices such as the SSC or DVR shown in [9]. This controller not only has function of controlling the voltage like STATCOM, but also has the potential of power flow control and damping out the power fluctuation, so recovery from the fault disturbance is very much faster. With prominent characteristics, a

LCC HVDC system combined with DVR will be presented in this thesis. And the proposed system will be comprehensively analyzed during under normal and fault conditions.

The thesis describes a control strategy for dynamic voltage restorer (DVR) comprising a static compensator (STATCOM) and a static series compensator (SSC) to regulate generated power from a large wind farm into the LCC HVDC system with special consideration of onshore grid fault. This is achieved through voltage modulation on the offshore network via the DVR. The mathematical analysis and the control design are verified through PSCAD simulation.

- Under normal operation conditions, the task of the STATCOM is to control the offshore system as an infinite source. It maintains the AC voltage, frequency and phase angle at constant values. The offshore AC voltage amplitude is regulated by output voltage amplitude of the STATCOM.
- Under grid fault conditions, fast reduction control of power generated from the wind farm must be activated. The STATCOM is used to lower the wind park network, so the power reduction is automatically effected. Meanwhile, the DVR uses a series-connected topology to generate a controllable voltage to against the short-term voltage reduction caused by the STATCOM. Consequently, the voltage at the local AC bus is always kept at a constant rated value and the commutation failure of the HVDC rectifier is prevented from. Therefore, the local load will be still supplied the power and LCC-HVDC system will transmit power to onshore grid.

This thesis contains five chapters. Chapter one briefly introduces new trends in power transmission from the wind farms. New ideas of this thesis are also compared with these of other studies in this chapter.

In chapter two, different topologies of shunt and series voltage compensators for mitigating voltage dips are presented and analyzed.

Chapter three considers a control solution for integration of large offshore DFIG based wind farms with a common collection bus, controlled by the DVR, into the main onshore grid, using LCC HVDC connection.

In chapter four, the simulation results of the proposed system are presented and analyzed.

Finally, in chapter five the conclusions of the thesis are given and future work is envisaged.

2. Voltage compensation in the wind farm

2.1 Shunt compensator for mitigating voltage dips

The grid is assumed stiff enough compared with the load. The grid and all transformers above the bus to which the STATCOM is connected can be represented by an ideal voltage source in series with equivalent impedance. Thus, the topology of the power system with STATCOM can be simplified as the system scheme of STATCOM for voltage dip mitigation, as presented in Fig. 2.1

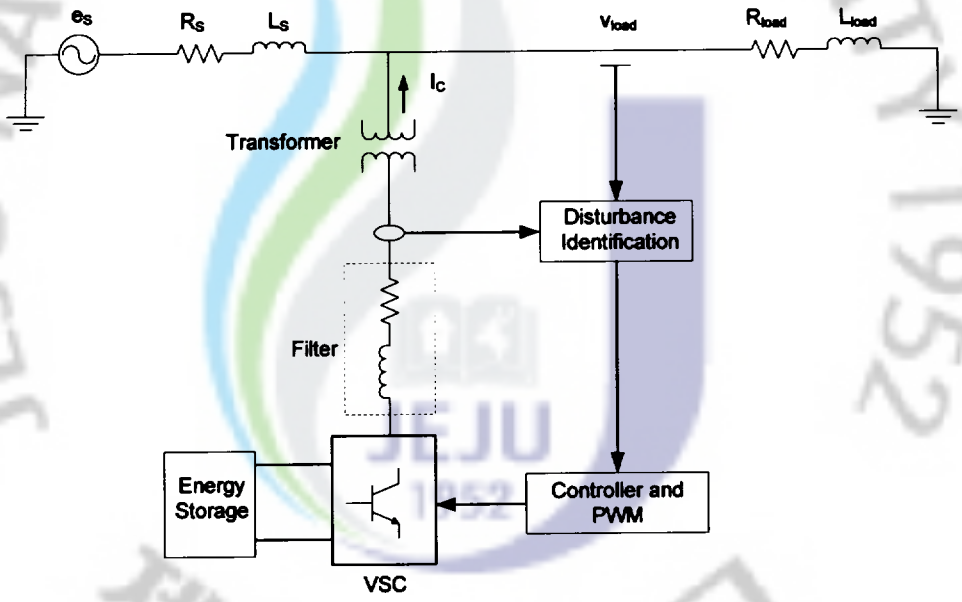

Fig. 2.1 System scheme of STATCOM for voltage dip mitigation.

As displayed in Figure 2.1, the STATCOM is composed of

- Three-phase VSC.

VSC is the core component of the STATCOM. During voltage dips, VSC generates proper voltages and introduces a voltage difference between the VSC and the point of connection with the power system. This voltage difference results in proper current that is injected into the power system. Active and reactive power can be injected independently in the power system.

- Energy storage.

The purpose of energy storage is to maintain the DC side voltage of VSC. It can be capacitor or DC source, e.g. battery. Traditional STATCOM only has DC capacitor.

Thus, only reactive power can be injected to the power system by STATCOM whereas both active and reactive power can be injected to the power system by STATCOM if DC source is used.

- Filter.

As the Pulse-Width Modulation (PWM) technique is used in VSC, the output voltage of VSC has switching ripple, which bring harmonics into the current injected to the power system. These harmonics will affect the voltage quality of the power system. Therefore, a relatively small reactor is installed between VSC and the point of the system, with which the STATCOM is connected, to filter those harmonics in the current. The filter can be small if high switching frequency is used.

- Controller.

The controller executes the calculation of the correct output voltage of VSC, which leads to proper shunt compensation current, and PWM modulation. VSC and controller will be illustrated in detail in Chapter 3.

2.2 Series compensator for mitigating voltage dips

The dynamic voltage restorer is a series connected device, which by voltage injection can control the load voltage. In the case of a voltage dip the DVR injects the missing voltage and it avoids any tripping the load. Fig. 2.2 illustrates the operation principle of a DVR.

The DVR is still very rarely inserted in the grid and only relative few devices have been inserted around the world. Most of the described projects include limited information about potential problems and a detailed description of the design and control aspects.

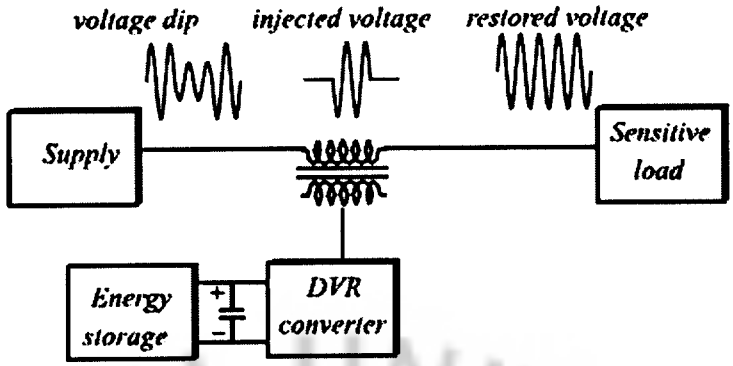

Fig. 2.2 Operation principle of a DVR.

Even though the DVR is commercially available today, the DVR is not a matured technology and several areas regarding the design and control of this type of device are at the basic research level. The design of a DVR has been treated in [11] with focus on the sizing of the voltage, power and current rating.

Additionally, the DVR is a series connected device and one of the drawbacks with series connected devices is the difficulties to protect the device during short circuits and avoid interference with the existing protection equipment.

2.2.1 Topologies to have active power access during voltage dips

During a voltage dip the DVR injects voltages and thereby restores the supply voltages. In this phase the DVR exchanges active and reactive power with the surrounding system. If active power is supplied to the load by the DVR, it needs a source for the energy. Two concepts are here considered, one concept uses stored energy and the other concept uses no significant energy storage. The stored energy can be delivered from different kinds of energy storage systems such as batteries, double-layer-capacitors, super-capacitors, flywheel storage or SMES. In the no-storage DVR concept, the DVR has practically no energy storage and the energy is taken from the remaining supply voltage during the voltage dip. The four system topologies, which are presented and compared are:

- Topologies with stored energy topologies

– Constant DC-link voltage.

– Variable DC-link voltage.

• Topologies with power from the supply

– Supply side connected passive shunt converter.

– Load side shunt connected passive shunt converter.

2.2.1.1 Topologies with stored energy

■ **Constant DC-link voltage**

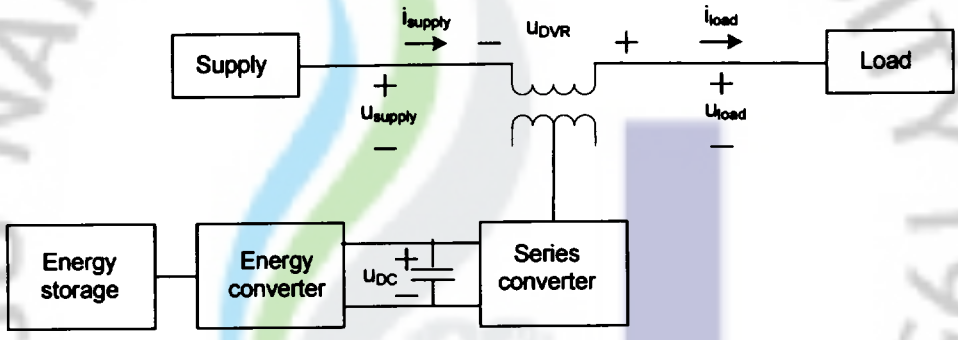

Fig. 2.3 DVR topology with power from stored energy and operating with constant DC-link voltage.

■ **Variable DC-link voltage**

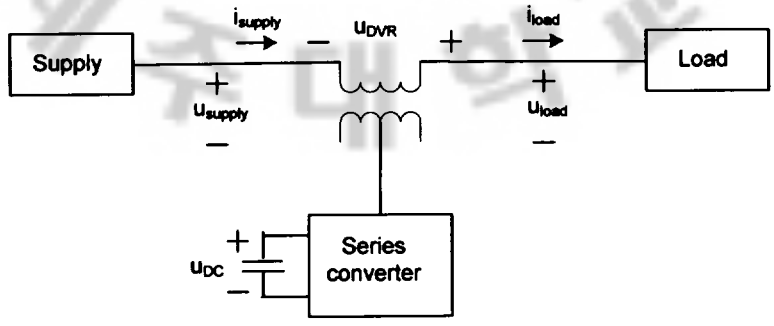

Fig. 2.4 DVR topology with power from stored energy and operating with variable DC-link voltage.

In this case all the energy is stored before the voltage dip and a very small scale converter is expected to be used to re-charge the energy storage. Two different control/hardware methods have been considered, which are a DVR operating with a constant DC-link voltage and a DVR operating with a variable DC-link voltage.

2.2.1.2 Topologies with power from the supply

Taking power from the remaining supply voltage has the disadvantage of an increase in the supply current. The advantages are cost saving of the energy storage and the ability to compensate long duration voltage dips.

■ **Supply side connected passive converter**

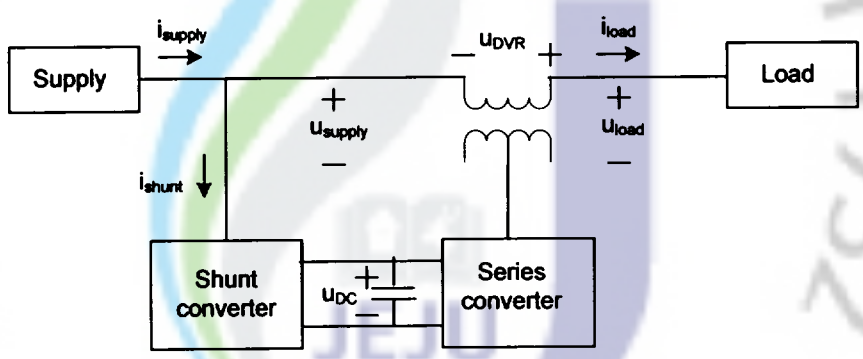

Fig. 2.5 DVR topology with energy from the grid and with a shunt converter at the supply side of the series converter.

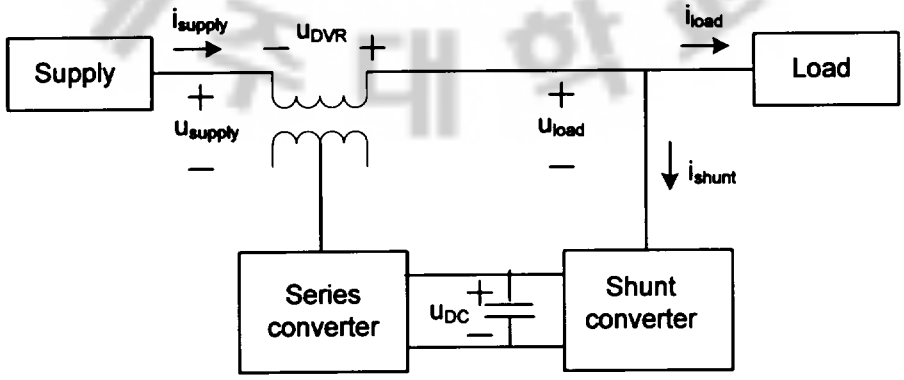

Fig. 2.6 DVR topology with energy from the grid and with the DVR operating with a shunt converter at the load side of the series converter.

Taking power from the grid can have a negative influence on the neighboring upstream loads, because the DVR protects its downstream loads by taking more current from the supply, which can lead to an even more severe voltage dip for upstream loads.

Topologies for DVR using power from the grid can generally be characterized with the location of the shunt converter at the supply side of the series converter or at the load side of the series converter. Both passive and active shunt converters can be used. Here, only passive diode converters are considered in a six pulse coupling, which are rated for full power transfer. This will give simple topologies, but passive solutions with diodes are less controllable and absorb non-linear currents.

Considering stationary conditions and active power only, the supply currents increase at a severe dip, because the active power to the load has to be supplied from the supply.

2.2.2 Comparison of the topologies for active power access

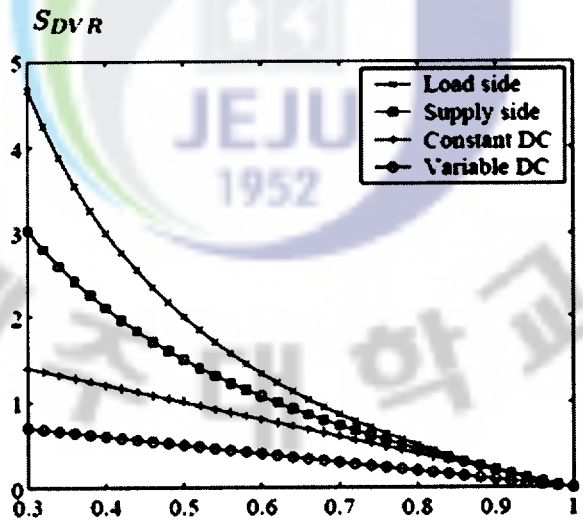

Fig. 2.7 Power rating of the converters used for the four topologies versus voltage dip size in p.u.

In this section a small comparison of the four DVR topologies has been performed. Fig. 2.7 illustrates how the rating of the converters varies with dip size for the four topologies. The load side connected converter requires the highest rated DVR followed by the supply side connected converter, constant DC and variable DC. To be able to compensate a load of 1 p.u. from a 0.5 p.u .voltage dip the four solutions require at least an installed rating of 0.5 p.u., 1 p.u., 1.5 p.u. or 2 p.u., respectively.

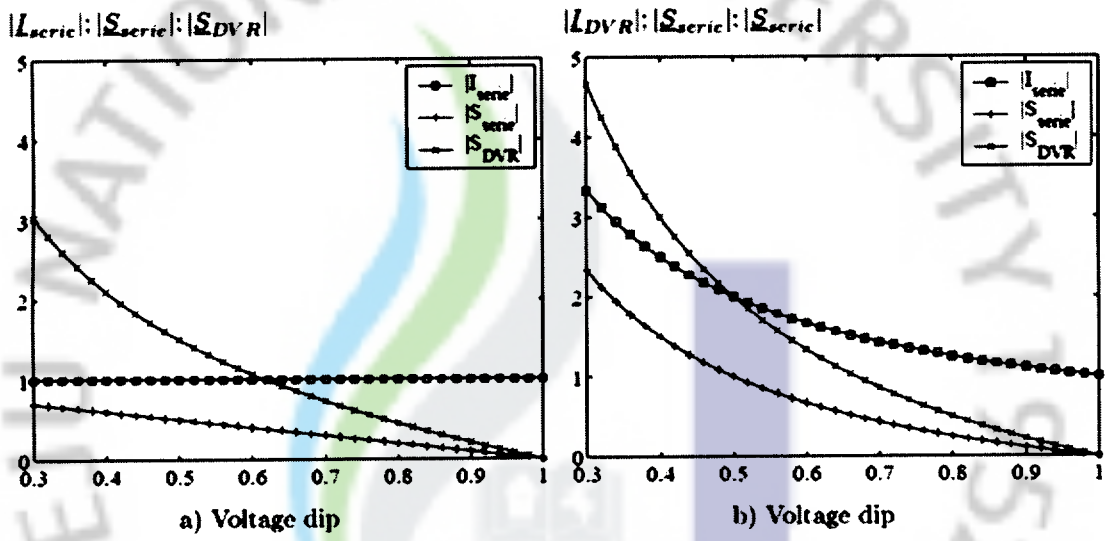

Fig. 2.8 Comparison of DVR topologies with power from the supply. The current requirements for the series converter ($|\underline{i}_{series}|$) power requirements for the series converter |($|\underline{s}_{series}|$)and the total DVR power requirements ($|\underline{s}_{DVR}|$) versus voltage dip size in p.u. a) supply side shunt converter and b) load side shunt converter.

In Fig. 2.8a and Fig. 2.8b the two topologies with power from the supply are compared. It includes the current rating of the series converter, power rating of the series converter and the total DVR rating versus voltage dip size. A difference exists in the rating of the series converter for the two concepts. For example, at 0.4 voltage dip the current through the series converter is 2.5 p.u. for the load side converter and 1 p.u. for the supply side. The associated power ratings for the series converter at this dip size are 0.6 and 1.5, respectively.

Table 2.1 Comparison of the different DVR topologies with the gradings: very good(++), good(+), poor(-) and very poor (- -).

	Stored Energy		No Stored Energy	
	Constant DC-link voltage	Variable DC-link voltage	Supply side connected converter	Load side connected converter
Long voltage dip duration	-	--	++	++
Deep voltage dips	++	-	--	+
Non-symmetrical voltage dips	++	++	--	+
DC-link voltage control	++	-	--	+
Size of energy storage	++	+		
Grid effects	+	+	--	-
Rating of charging/shunt converter	--	+	--	-
Rating of the series converter	+	+	+	--
System complexity	-	++	+	+
Cost Estimation	--	-	+	+
Control complexity	-	-	++	+
Sum (+)	10	8	6	8
Sum (-)	7	6	10	4
Sum (total)	3	2	-4	4

Table 2.1 illustrates the different topologies and a four level rating of each topology is done. Although the best topology cannot be ultimately stated, some main differences can be seen. In this comparison the system with a load side connected shunt converter is estimated to have the highest total points with general high performance followed with low cost and complexity. Still the negative grid effects and high rated series converter could disqualify the solution for certain applications.

3. Control design of the proposed system

3. 1 System Configuration

The grid voltage control system configuration is shown in Fig. 3.1.

The task of the STATCOM is to control the offshore system as an infinite source. It maintains the AC voltage, frequency and phase angle at constant values. The offshore AC voltage amplitude is regulated by output voltage amplitude of the STATCOM.

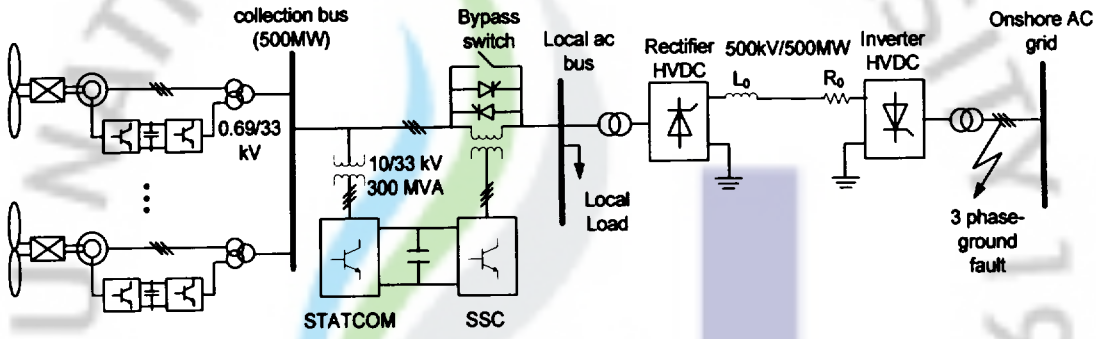

Fig. 3.1 Power system to be studied.

In steady state operation, the total active power delivered by all DFIGs must balance the power transferred to the HVDC link, consumed by local loads, and dissipated as losses. Any imbalance will cause the STATCOM DC-link voltage to vary. Therefore, the STATCOM capacitor voltage can be regarded as an immediate indicator of active power imbalance and can be used for fast adjustment of HVDC DC-link current reference.

Under disturbance conditions such as a balanced onshore main fault, wind gust, or wind speed over its rated limit of generator, surplus power on the offshore network rapidly builds up as the wind farm is not aware of the condition and continues to generate power, which absorbed by the STATCOM capacitor. To prevent the STATCOM DC voltage from going out of control and the system from tripping, the wind farm power must be reduced as soon as possible.

To do this, a method is based on the idea that by lowering the wind park network voltage at the collection bus via the STATCOM a power reduction is automatically effected. A reduction of the wind park voltage amplitude must comply with the Grid Code shown in [10]. In accordance with the Grid Code, fault ride through (FRT) requirements are described based on a time voltage diagram in Fig. 3.2 which does not contain characteristic voltage behavior but border lines. Meanwhile, the DVR uses a series-connected topology to generate a controllable voltage to against the short-term voltage reduction caused by the STATCOM, this means that the voltage at the local AC bus always keep at a constant rated value.

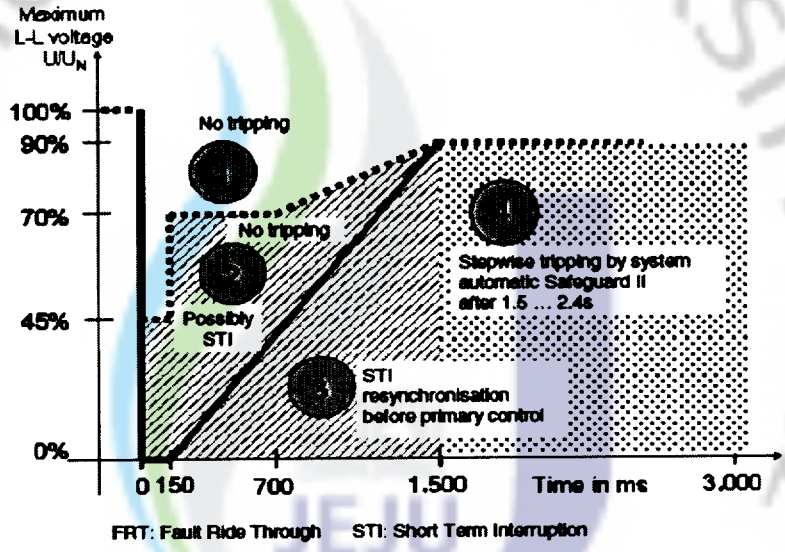

Fig. 3.2 Definition of FRT requirements.

3. 2 System model for control design

The total system of multiple DFIGs, their converter controls, the STATCOM, local loads, transformers, and HVDC rectifier-inverter system, is highly complex. To simplify the model for control design, some assumptions are made.

- Multiple DFIGs can be aggregated into a single DFIG of appropriate rating.
- For the purpose of local AC grid (collector bus) and power tracking control, the aggregated DFIG is considered as a controlled current source.

- The AC harmonic filters are designed to suppress 11th, 13th, and higher harmonics, and have natural frequencies above the designed control system bandwidths. For control purposes, the filters are represented by their dominant low frequency capacitive properties.
- Power losses in the STATCOM and HVDC rectifier are ignored.
- The HVDC inverter is in the voltage-control mode, and under normal conditions has little effect on the collector grid control regimes. It is replaced by an equivalent DC voltage source.

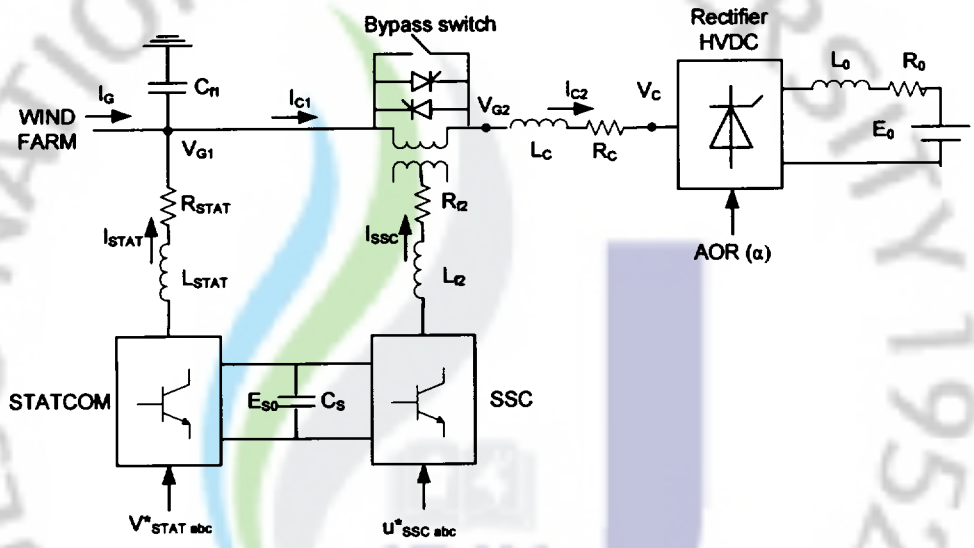

Fig. 3.3 Simplified diagram of the system studied.

Under these assumptions, the system is shown in Fig. 3.3. The DFIGs deliver current I_G to the local AC bus, while the HVDC link absorbs current I_{C1} or I_{C2} in normal or fault operation conditions respectively. Capacitor C_{fl} corresponds to the total capacitance of the harmonic filters installed on the local bus. Passive RL elements represent the transformers and cable parameters. Depending on operational demands, the STATCOM current I_{STAT} can be injected to, or absorbed from, the local bus. The parameters R_0, L_0 represent the HVDC dc-link connection. The cable capacitance is neglected for control design. The dc voltage source E_0 replaces the HVDC inverter under voltage control as assumed earlier.

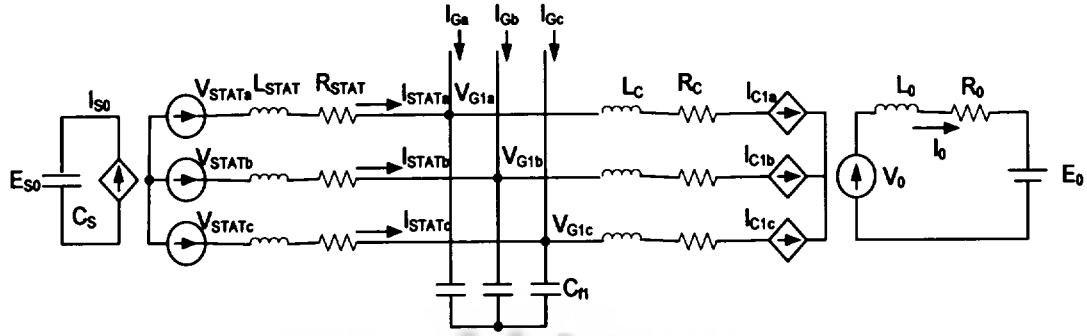

Fig. 3.4 Equivalent circuit of the proposed system for mathematical modeling under normal operation condition.

The plant equations are derived from the equivalent circuit shown in Fig. 3. 4. Seen from the collector grid, the HVDC rectifier is a current source dependent on the collector grid voltage. Seen from the DC side, the rectifier can be considered as a voltage source with magnitude $V_0 \approx k_r V_{G1} \cos \alpha$ where k_r is a constant defined by rectifier scheme. The STATCOM is a voltage source converter and is represented as a three-phase voltage source V_{STAT} causing current I_{STAT} flow to/from the local grid. The STATCOM DC-side has current-source properties derived from the current I_{STAT} transformed into the DC-current I_{S0}. The equivalent circuit in Fig. 3.4 assumes that all the system parameters are referred to the local DC bus.

In Fig. 3.3, it can be seen the electro-mechanical bypass and the thyristor crow-bar, responsible for conduction of the load currents in the absence of disturbances in the utility grid voltage. The crow-bar thyristors also provide a fast bypass protection against short-circuits at the load side. Therefore, under normal operation conditions, the DVR only uses the STATCOM.

3. 2. 1 System model under normal operation condition

The equations derived from Fig. 3.3 and 3.4 can be conditionally partitioned into three parts representing local ac bus, STATCOM DC link, and HVDC DC link. The local AC bus equations are

$$\left.\begin{aligned} L_{STAT}\frac{dI_{STAT}}{dt} &= -R_{STAT}I_{STAT} + V_{STAT} - V_{G1} \\ C_{f1}\frac{dV_{G1}}{dt} &= I_{STAT} + I_G - I_{C1} \\ L_C\frac{dI_{C1}}{dt} &= -R_C I_{C1} + V_{G1} - V_C \end{aligned}\right\} \quad (3.1)$$

Where I_{STAT}, I_G, I_{C1}, and V_{G1} are three-phase current and voltage vectors ($I_{STAT} = [I_{STATa}\ I_{STATb}\ I_{STATc}]^T$, etc.). Equation (3.1) comprises nine equations: three equations for each phase a, b, and c. The number of equations can be reduced by transformation of (3.1) into the synchronously rotating reference dq frame to give

$$\left.\begin{aligned} L_{STAT}\frac{dI_{STATd}}{dt} &= -R_{STAT}I_{STATd} + V_{STATd} - V_{G1d} + \omega L_{STAT}I_{STATq} \\ L_{STAT}\frac{dI_{STATq}}{dt} &= -R_{STAT}I_{STATq} + V_{STATq} - V_{G1q} - \omega L_{STAT}I_{STATd} \\ C_{f1}\frac{dV_{G1d}}{dt} &= I_{STATd} + I_{Gd} - I_{C1d} + \omega C_{f1}V_{G1q} \\ C_{f1}\frac{dV_{G1q}}{dt} &= I_{STATq} + I_{Gq} - I_{C1q} - \omega C_{f1}V_{G1d} \end{aligned}\right\} \quad (3.2)$$

$$\left.\begin{aligned} L_C\frac{dI_{C1d}}{dt} &= -R_C I_{C1d} + V_{G1d} - V_{Cd} + \omega L_C I_{C1q} \\ L_C\frac{dI_{C1q}}{dt} &= -R_C I_{C1q} + V_{G1q} - V_{Cq} - \omega L_C I_{C1d} \end{aligned}\right\} \quad (3.3)$$

Where α is an electrical frequency of the rotating dq frame. Note that the number of equations (six) corresponds to the number of mesh loops in the AC part of the circuit depicted in Fig. 3.3.

The STATCOM's dc-link equation can be derived from power balance condition:

$$P_{STAT} = I_{S0}E_{S0} = \frac{3}{2}\left(V_{STATd}I_{STATd} + V_{STATq}I_{STATq}\right) \quad (3.4)$$

using $I_{S0} = C_S\frac{dE_{S0}}{dt}$, the following can be written:

$$C_S\frac{dE_{S0}^2}{dt} = \frac{3}{2}\left(V_{STATd}I_{STATd} + V_{STATq}I_{STATq}\right) \quad (3.5)$$

Since there must be a balance of active power, the power to STATCOM can be expressed in terms of power P_G generated by DFIGs and power P_C converted to HVDC. Therefore, (3.5) can be given:

$$C_S \frac{dE_{S0}^2}{dt} = 2P_{STAT} = 2P_G - 2P_C \tag{3.6}$$

which confirms that the STATCOM capacitor voltage is an indicator of the power balance between the wind farm and the HVDC link.

From Fig. 3.4, the HVDC rectifier dc current is given by

$$L_0 \frac{dI_0}{dt} = -R_0 I_0 + V_0 - E_0, \; V_0 = k_r \sqrt{V_{Cd}^2 + V_{Cq}^2} cos\alpha \tag{3.7}$$

Where α is the firing angle of the rectifier bridge. For a 12-pulse rectifier used in typical HVDC systems, $k_r = 6\sqrt{2}/\pi \approx 2.7$. Using the rectifier active and reactive power linkage $Q_C = P_C \tan \alpha$, and balancing the active power, one can derive two equations linking converter current components I_{C1d} and I_{C1q}:

$$\left.\begin{aligned} V_{Cd} I_{C1d} + V_{Cq} I_{C1q} &= \frac{2}{3} k_r \sqrt{V_{Cd}^2 + V_{Cq}^2}\, I_0 \cos\alpha \\ V_{Cd} I_{C1q} - V_{Cq} I_{C1d} &= \frac{2}{3} k_r \sqrt{V_{Cd}^2 + V_{Cq}^2}\, I_0 \sin\alpha \end{aligned}\right\} \tag{3.8}$$

So that the rectifier currents drawn from the local collector bus are:

$$\left.\begin{aligned} I_{C1d} &= \frac{2}{3} k_r I_0 \left(\frac{V_{Cd}}{\sqrt{V_{Cd}^2 + V_{Cq}^2}} cos\alpha - \frac{V_{Cq}}{\sqrt{V_{Cd}^2 + V_{Cq}^2}} sin\alpha \right) \\ I_{C1q} &= \frac{2}{3} k_r I_0 \left(\frac{V_{Cq}}{\sqrt{V_{Cd}^2 + V_{Cq}^2}} cos\alpha + \frac{V_{Cd}}{\sqrt{V_{Cd}^2 + V_{Cq}^2}} sin\alpha \right) \end{aligned}\right\} \tag{3.9}$$

To complete the HVDC rectifier model, (3.9) should be accompanied by equations for voltage at the converter terminals V_C

$$\left.\begin{aligned} V_{Cd} &= V_{G1d} - R_C I_{Cd} - L_C \frac{dI_{Cd}}{dt} + \omega L_C I_{Cq} \\ V_{Cq} &= V_{G1q} - R_C I_{Cq} - L_C \frac{dI_{Cq}}{dt} - \omega L_C I_{Cd} \end{aligned}\right\} \tag{3.10}$$

Substitution of (3.9) into (3.10), together with (3.7), results in a complex system of nonlinear differential equations describing the interaction between the HVDC rectifier and the local bus. In such a form, the set of equations cannot be useful for control design. However, if (3.8)

and (3.9) are written in a synchronously rotating reference frame aligned on the rectifies ac-terminal voltage (i.e., V_{Cq}=0), the relation between I_{C1d}, I_{C1q}, and I_0 can be derived in a straightforward manner

$$\left.\begin{aligned} I_{C1d} &= \frac{2}{3}k_r I_0 cos\alpha \\ I_{C1q} &= \frac{2}{3}k_r I_0 sin\alpha \end{aligned}\right\} \tag{3.11}$$

Substitution of (3.11) into (3.6), together with (3.7), results in

$$C_S \frac{dE_{S0}^2}{dt} = 2P_G - 2P_C = 3V_{G1d}I_{Gd} - 2k_r I_0 V_{G1d} cos\alpha \tag{3.12}$$

$$L_0 \frac{dI_0}{dt} = -R_0 I_0 + k_r V_{G1d} cos\alpha - E_0 \tag{3.13}$$

Summarizing, the entire plant described by mathematical model under normal operation condition is given by equations (3.2), (3.12) and (3.13). Therefore, the final control system structure is shown in Fig. 3.5 below.

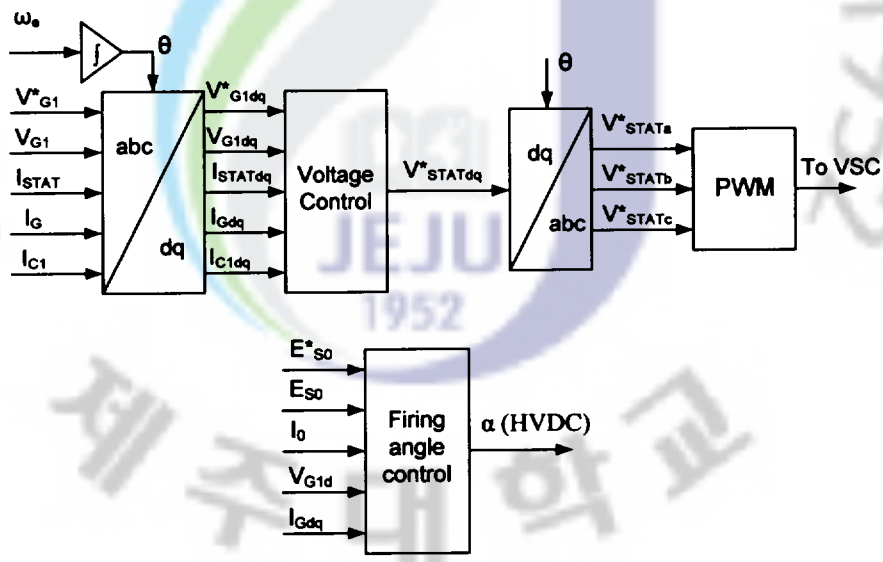

Fig. 3.5 STATCOM and HVDC control block diagram.

3. 2. 2 System model under fault condition

HVDC current is maintained at 0.25 p.u. level using switch S in Fig. 3.6. Following the fault, the switch is changed to the F mode. When the fault is cleared, the control is switched

back to the normal operation.

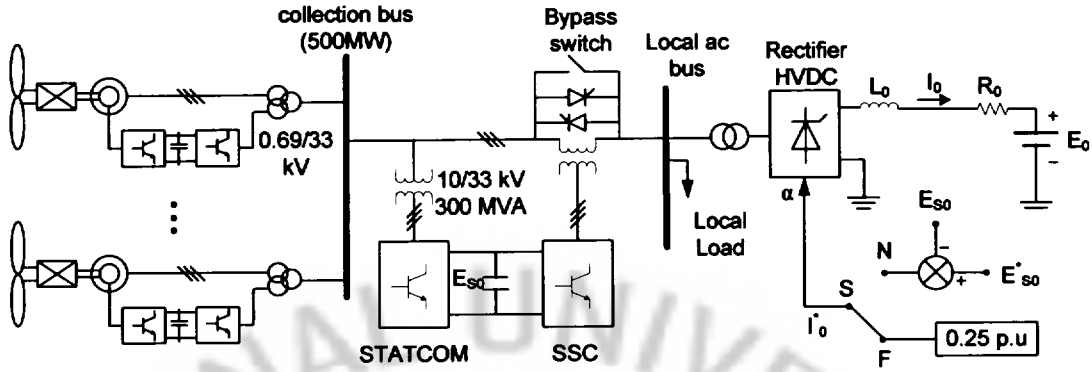

Fig. 3.6 System model under fault conditions at onshore grid.

Under the disturbance conditions, wind farm network voltage at the collection bus is fast lowered via the STATCOM control to regulate generated power for preventing from break-down of whole power system. Therefore, voltage dips will appear at the local bus, and this negatively impact on local power system as well as the supplying power to local load; especially on commutation failure of the rectifier of the HVDC system.

To solve this problem, the DVR will use the SSC to generate a controllable voltage to against the voltage dips, and so it will keep the local bus voltage at a rated constant value.

3.2.2.1 Proportional Controller for the SSC

A three-phase model of the LC-filter, derived from Fig. 3.8, is transformed into the dq-coordinate system, where the d-axis is oriented with the grid flux vector.

The equations derived from Fig. 3.8.

$$\left.\begin{aligned} u_{SSC}(t) &= u_C(t) + R_{f2} i_{SSC}(t) + L_{f2}\frac{di_{SSC}(t)}{dt} \\ i_{SSC}(t) &= i_{C1}(t) + C_{f2}\frac{du_C(t)}{dt} \end{aligned}\right\} \quad (3.14)$$

Where $i_{SSC}(t)$, $i_{C1}(t)$, $u_{SSC}(t)$, and $u_C(t)$ are three-phase current and voltage vectors ($i_{SSC}(t) = [i_{SSCa}(t)\ i_{SSCb}(t)\ i_{SSCc}(t)]^T$, etc.).

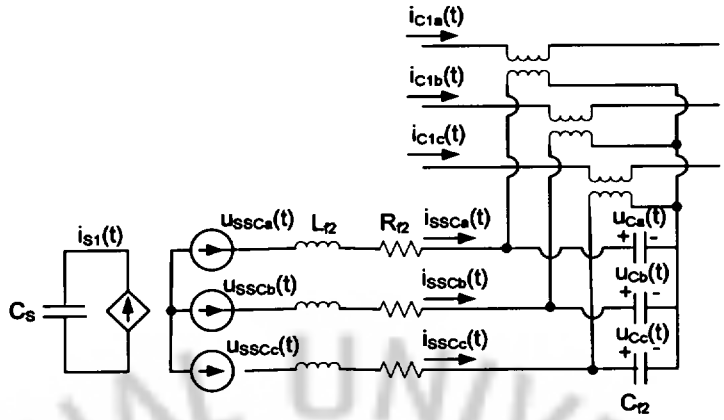

Fig. 3.7 Overview of the SSC.

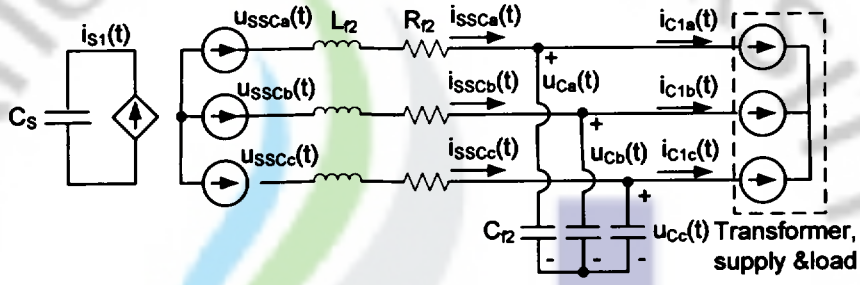

Fig. 3.8 Simplified scheme of the SSC used to derive controller.

Equation (3.14) comprises six equations: three equations for each phase a, b, and c. The number of equations can be reduced by transformation of (3.14) into the synchronously rotating reference d-q frame to give

$$\left.\begin{aligned} u_{SSCd}(t) &= u_{Cd}(t) + R_{f2}i_{SSCd}(t) + L_{f2}\frac{di_{SSCd}(t)}{dt} - \omega L_{f2}i_{SSCq}(t) \\ u_{SSCq}(t) &= u_{Cq}(t) + R_{f2}i_{SSCq}(t) + L_{f2}\frac{di_{SSCq}(t)}{dt} + \omega L_{f2}i_{SSCd}(t) \end{aligned}\right\} \quad (3.15)$$

$$\left.\begin{aligned} i_{SSCd}(t) &= i_{C1d}(t) - \omega C_{f2}u_{Cq}(t) + C_{f2}\frac{du_{Cd}(t)}{dt} \\ i_{SSCq}(t) &= i_{C1q}(t) + \omega C_{f2}u_{Cd}(t) + C_{f2}\frac{du_{Cd}(t)}{dt} \end{aligned}\right\} \quad (3.16)$$

The vector current controller is implemented in the computer. Thus, the voltages and currents are sampled with the constant sample time T_S. The equivalent inductance and the resistance of the LC-filter are denoted as L_{f2}, C_{f2} and R_{f2}, which mean these are predicted values.

These equations (3.15) and (3.16) is discretized using forward Euler method and is then

integrated from kT_S to $(k+1)T_S$ (one sample period).

$$\left.\begin{aligned}
\int_{kT_S}^{(k+1)T_S} u_{SSCd}(t)dt &= \int_{kT_S}^{(k+1)T_S} u_{Cd}(t)dt + \int_{kT_S}^{(k+1)T_S} R_{f2} i_{SSCd}(t)dt \\
&\quad + \int_{kT_S}^{(k+1)T_S} L_{f2} \frac{di_{SSCd}(t)}{dt} dt - \int_{kT_S}^{(k+1)T_S} \omega L_{f2} i_{SSCq}(t)dt \\
\int_{kT_S}^{(k+1)T_S} u_{SSCq}(t)\,dt &= \int_{kT_S}^{(k+1)T_S} u_{Cq}(t)\,dt + \int_{kT_S}^{(k+1)T_S} R_{f2} i_{SSCq}(t)dt \\
&\quad + \int_{kT_S}^{(k+1)T_S} L_{f2} \frac{di_{SSCq}(t)}{dt} dt + \int_{kT_S}^{(k+1)T_S} \omega L_{f2} i_{SSCd}(t)\,dt
\end{aligned}\right\} \quad (3.17)$$

$$\left.\begin{aligned}
\int_{kT_S}^{(k+1)T_S} i_{SSCd}(t)dt &= \int_{kT_S}^{(k+1)T_S} i_{C1d}(t)dt - \int_{kT_S}^{(k+1)T_S} \omega C_{f2} u_{Cq}(t)dt \\
&\quad + \int_{kT_S}^{(k+1)T_S} C_{f2} \frac{du_{Cd}(t)}{dt} dt \\
\int_{kT_S}^{(k+1)T_S} i_{SSCq}(t)dt &= \int_{kT_S}^{(k+1)T_S} i_{C1q}(t)dt + \int_{kT_S}^{(k+1)T_S} \omega C_{f2} u_{Cd}(t)dt \\
&\quad + \int_{kT_S}^{(k+1)T_S} C_{f2} \frac{du_{Cd}(t)}{dt} dt
\end{aligned}\right\} \quad (3.18)$$

Equation (3.17) and (3.18) are divided by T_S to obtain the average value for the sample period k to k+1

$$\left.\begin{aligned}
u_{SSCd}(k,k+1) &= u_{Cd}(k,k+1) + R_{f2} i_{SSCd}(k,k+1) \\
&\quad + \frac{L_{f2}}{T_S}\left[di_{SSCq}(k+1) - di_{SSCq}(k)\right] - \omega L_{f2} i_{SSCq}(k,k+1) \\
u_{SSCq}(k,k+1) &= u_{Cq}(k,k+1) + R_{f2} i_{SSCq}(k,k+1) \\
&\quad + \frac{L_{f2}}{T_S}\left[di_{SSCq}(k+1) - di_{SSCq}(k)\right] + \omega L_{f2} i_{SSCd}(k,k+1)
\end{aligned}\right\} \quad (3.19)$$

$$\left.\begin{aligned}
i_{SSCd}(k,k+1) &= i_{C1d}(k,k+1) - \omega C_{f2} u_{Cq}(k,k+1) \\
&\quad + \frac{C_{f2}}{T_S}\left[u_{Cd}(k+1) - u_{Cd}(k)\right] \\
i_{SSCq}(k,k+1) &= i_{C1q}(k,k+1) + \omega C_{f2} u_{Cd}(k,k+1) \\
&\quad + \frac{C_{f2}}{T_S}\left[u_{Cq}(k+1) - u_{Cq}(k)\right]
\end{aligned}\right\} \quad (3.20)$$

The following assumptions are made to derive the controller:

- The grid current $i_{C1dq}(t)$ is constant independently of variations in currents and voltages of the LC-filter.
- The capacitor voltage $u_{Cdq}(t)$ and the inductor current $i_{SSCdq}(t)$ change linearly during one sample period.
- The average values of the capacitor voltage $u_{Cdq}(t)$ and the inductor current $i_{SSCdq}(t)$ over the sample period kT_S to $(k+1)T_S$ are each equal to the half sum of the real value and the reference value at sample k.
- The average values of the voltages $u_{SSCdq}(t)$ and currents $i_{SSCdq}(t)$ during one period are assumed to equal the reference voltages and currents respectively, which are denoted as $u^*_{SSCdq}(t)$ and $i^*_{SSCdq}(t)$.

Based on the above assumptions, the equations (3.19) and (3.20) of the proportional controller are obtained as:

$$\left.\begin{aligned} u^*_{SSCd}(k) &= u^*_{Cd}(k) + R_{f2}i_{SSCd}(k) - \frac{\omega L_{f2}}{2}\{i^*_{SSCq}(k) + i_{SSCq}(k)\} \\ &\quad + k_p\{i^*_{SSCd}(k) - i_{SSCd}(k)\} \\ u^*_{SSCq}(k) &= u^*_{Cq}(k) + R_{f2}i_{SSCq}(k) + \frac{\omega L_{f2}}{2}\{i^*_{SSCd}(k) + i_{SSCd}(k)\} \\ &\quad + k_p\{i^*_{SSCq}(k) - i_{SSCq}(k)\} \end{aligned}\right\} \quad (3.21)$$

$$\left.\begin{aligned} i^*_{SSCd}(k) &= i_{C1d}(k) - \frac{\omega C_{f2}}{2}\{u^*_{Cq}(k) + u_{Cq}(k)\} + K_u\{u^*_{Cd}(k) - u_{Cd}(k)\} \\ i^*_{SSCq}(k) &= i_{C1q}(k) + \frac{\omega C_{f2}}{2}\{u^*_{Cd}(k) + u_{Cd}(k)\} + K_u\{u^*_{Cq}(k) - u_{Cq}(k)\} \end{aligned}\right\} \quad (3.22)$$

where $u^*_{SSCd}(k)$, $u^*_{SSCq}(k)$, $i^*_{SSCd}(k)$ and $i^*_{SSCq}(k)$ are the required reference currents and voltages to track the reference voltage of the capacitor. The gains K_u and K_p are the dead-beat gains calculated in terms of the filter parameters and the sampling time; $K_u = C_f/T_S$, $K_p = L_f/T_S + R_f/2$.

3.2.2.2 Delayed Proportional Controller for the SSC

The reference voltage $u^*_{SSC}(k)$ of the controller is delayed one sample due to analog to digital conversion and computer calculation time. Therefore, to prevent oscillations, a time delay compensation term is introduced so that the proportional gain can be set to dead-beat. The compensation term, denoted by $\Delta \underline{u}^{dq}_{SSC}(k)$, deletes the error caused by the one-sample delay of the VSC voltage references and is calculated as:

$$\Delta \underline{u}^{dq}_{SSC}(k+1) = -\Delta \underline{u}^{dq}_{SSC}(k) + K_p\{\underline{i}^{*dq}_{SSC}(k) - \underline{i}^{dq}_{SSC}(k)\} \tag{3.23}$$

The voltage controller is thus the same as in case of proportional controller, given by (3.22). The delayed proportional current controller is given by:

$$\left.\begin{aligned} u^*_{SSCd}(k+1) &= u^*_{Cd}(k) + R_{f2} i_{SSCd}(k) - \frac{\omega L_{f2}}{2}\{i^*_{SSCq}(k) + i_{SSCq}(k)\} \\ &+ K_p\{i^*_{SSCd}(k) - i_{SSCd}(k)\} - \Delta u_{SSCd}(k) \\ u^*_{SSCq}(k+1) &= u^*_{Cq}(k) + R_{f2} i_{SSCq}(k) + \frac{\omega L_{f2}}{2}\{i^*_{SSCd}(k) + i_{SSCd}(k)\} \\ &+ K_p\{i^*_{SSCq}(k) - i_{SSCq}(k)\} - \Delta u_{SSCq}(k) \end{aligned}\right\} \tag{3.24}$$

To conclude, the equations (3.21), (3.22), (3.23) and (3.24) will establish a control method for the SSC shown in Fig. 3.9.

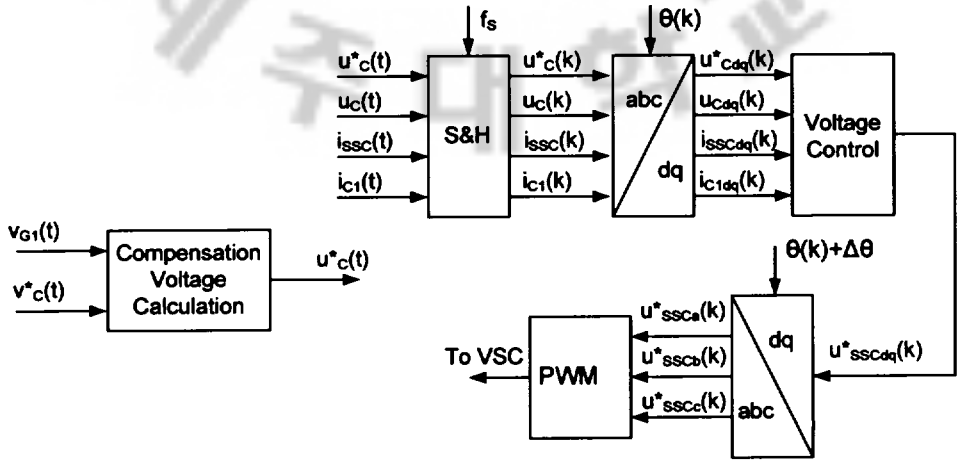

Fig. 3.9 SSC control block diagram.

4. Simulation results

4.1 Simulation conditions

A model of the proposed LCC HVDC system was created within EMTDC/PSCAD. It consists of a 500 MW wind farm using DFIG driven turbines which is connected to the main grid via a 500 MW, 500 kV LCC HVDC connection. The sending end of the HVDC system is modeled as 12-pulse rectifier (complete switching model) according to the CIGRE benchmark model [12] while the receiving end is a DC source 490 kV representing the HVDC inverter under voltage control. The DC-link connection is set at 80 km with parameters of a total resistance of 5 Ω and a total inductance of 1.836 H, but with the cable capacitance neglected. Rated HVDC link current is 1 kA. The model includes the HVDC step-up transformers and (300 MVA, 33/213 kV, 0.12 p.u. each), wind-farm step-up transformer (600 MVA, 0.69/33 kV, 0.12 p.u.), and the AC filters.

The DFIG-based wind farm is considered like a current source I_G, delivering power to the local collector bus. The offshore converter commutation voltage is supplied by a ± 300 MVA, six-pulse, VSC-based STATCOM with a DC capacitor of 40000 μF and a DC voltage of 30 kV. The converter switching frequency is 2500 Hz.

4.1.1 Normal operation

The control system should maintain collector grid voltage and frequency under continuously changing wind farm power. Fig. 4.1(a) simulation results show the response to a series of step changes in real power (1 p.u. → 0.7 p.u. → 0.4 p.u. → 0.7 p.u. → 1 p.u.) from the DFIG, which were implemented through steps in the currents I_{Gd}. Such step changes represent a worst case transient.

4.1.2 Fault condition

In each of the simulation results shown below, a three-phase-to-ground fault occurs on the onshore grid at 1 s and lasts for 150 ms. During a fault on the onshore network, causing the inverter terminal voltage to collapse, the inverter commutation will fail. This causes a short circuit on the DC side and collapse of the DC link voltage and transmitted power. Such a fault can be simulated in the model of Fig. 3.6 by setting $E_0 = 0$ for 150 ms duration (9 cycles at 60 Hz).

4.2 Analysis of simulation results

4.2.1 Normal operation

As shown in Fig. 4.1, generated power drops from 1 p.u. to 0.7 p.u. at 1.5s results in an increase of rectifier firing angle, the HVDC link delivering less active power and so the STATCOM DC-link voltage is kept at a constant rated level of 30 kV.

Fig. 4.1 clearly shows excellent regulation of the AC collector grid's voltage and frequency, and power balance via control of the STATCOM DC-link voltage.

4.2.2 Fault condition

4.2.2.1 Control system performance without the SSC

This section investigates the STATCOM performance for the control system following a short circuit fault in the onshore grid on the inverter side of the HVDC link.

As the fault occurs, the STATCOM starts to absorb the excess active power in the local bus, and its DC voltage increases as shown in Fig. 4.2. During the fault, the HVDC dc-link current is limited at 250% by hard limits on the demand. When the fault is cleared, the HVDC DC-link voltage recovers, the power transmission resumes, and after some transient, the STATCOM DC-link voltage returns to its rated value. The power coming from DFIGs is transferred to the HVDC again. The maximum STATCOM DC link voltage of 2.17 p.u. is a consequence of the constant DFIG output power.

After fault detection in a real system, generated power will be immediately reduced and DC-link voltage significantly reduced. Fig. 4.2 shows that system performance during a fault is stable and quite satisfactory for such a severe condition.

4.2.2.2 Control system performance without local load

Further tests on operation and performance of the system during a solid three-phase to ground fault on the grid side without local load at offshore grid were carried out. Before the fault, the generated and transmitted active power was around 1 p.u. and the STATCOM dc-link voltage was 30 kV (1 p.u.). As can be seen from Fig. 4.3 (a), the voltage at collection bus is lowered to 0.18 p.u. during fault via the STATCOM, which results in a reduction of (1 p.u. - 0.18 p.u. = 0.82 p.u.) in generated power as shown in Figure 4.3(e), and consequently the STATCOM DC-link voltage to just over 40 kV (1.35 p.u.) compared to its 2.17 p.u. in the previous case as shown in Fig. 4.3(g) and 4.2(c). The power reduction of 0.82 p.u. is chosen to simulate because it is easier to compare two cases of this section and next section 4.2.2.3 which a local load of 90 MW equal to generated power of 0.18 p.u. will be connected at the local bus.

Meanwhile a controllable voltage is generated from the SSC to keep local load voltage at a constant rated value as shown in Fig. 4.3(b, c), and consequently prevents from the commutation failure of the HVDC rectifier. The HVDC current is maintained at 0.25 p.u. level using switch S in Fig. 3.5 during the fault duration.

4.2.2.3 Control system performance with local load

This section presents the system model with a local load of 90 MW connected at the local bus. As the fault occurs, the firing angle increases to approximately 90 degrees to regulate

HVDC DC-link current to a setting value of 0.25 p.u. So power into the HVDC drops to almost zero as shown in Fig. 4.4(e).

Because local bus voltage always keep at a constant rated value via the SSC during the fault, the load is uninterruptedly supplied with enough power if rate of voltage reduction at collection bus is controlled so that generated power is equal to local load power and losses.

The reason for this is that as mentioned before, the total power delivered by all DFIGs must balance the power transferred to the HVDC link, consumed by local load, and dissipated as losses. Since the transmitted power to the HVDC is almost zero and the generated power regulated by lowering the collection bus voltage is equal to the local load power during the fault, the pink line presenting local load power shown in Fig. 4.4(e) is always constant during simulation period. On the other hand, because of the power balance, the STATCOM DC-link voltage is almost constant during the fault time as shown in Fig. 4.4(g) compared to the same case shown in Fig. 4.3(g).

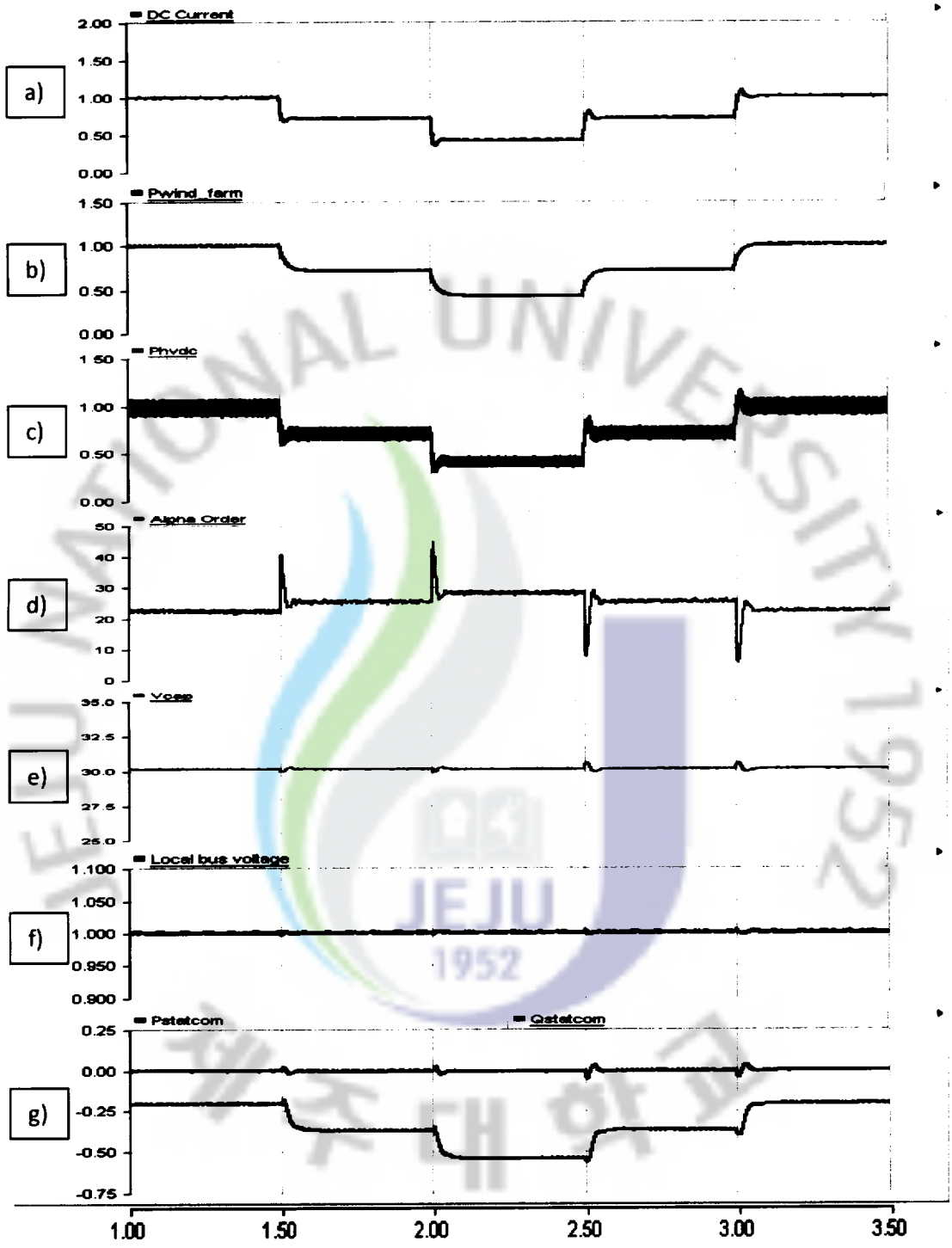

Fig. 4.1 Control system performance under normal operation.

a) HVDC DC-link current (p.u.). b) Active power generated from the wind farm (p.u.).

c) Active power transferred through HVDC (p.u.). d) Rectifier firing angle (degree).

e) STATCOM DC-link voltage (kV). f) Local bus voltage (p.u.).

g) STATCOM active and reactive power (p.u.).

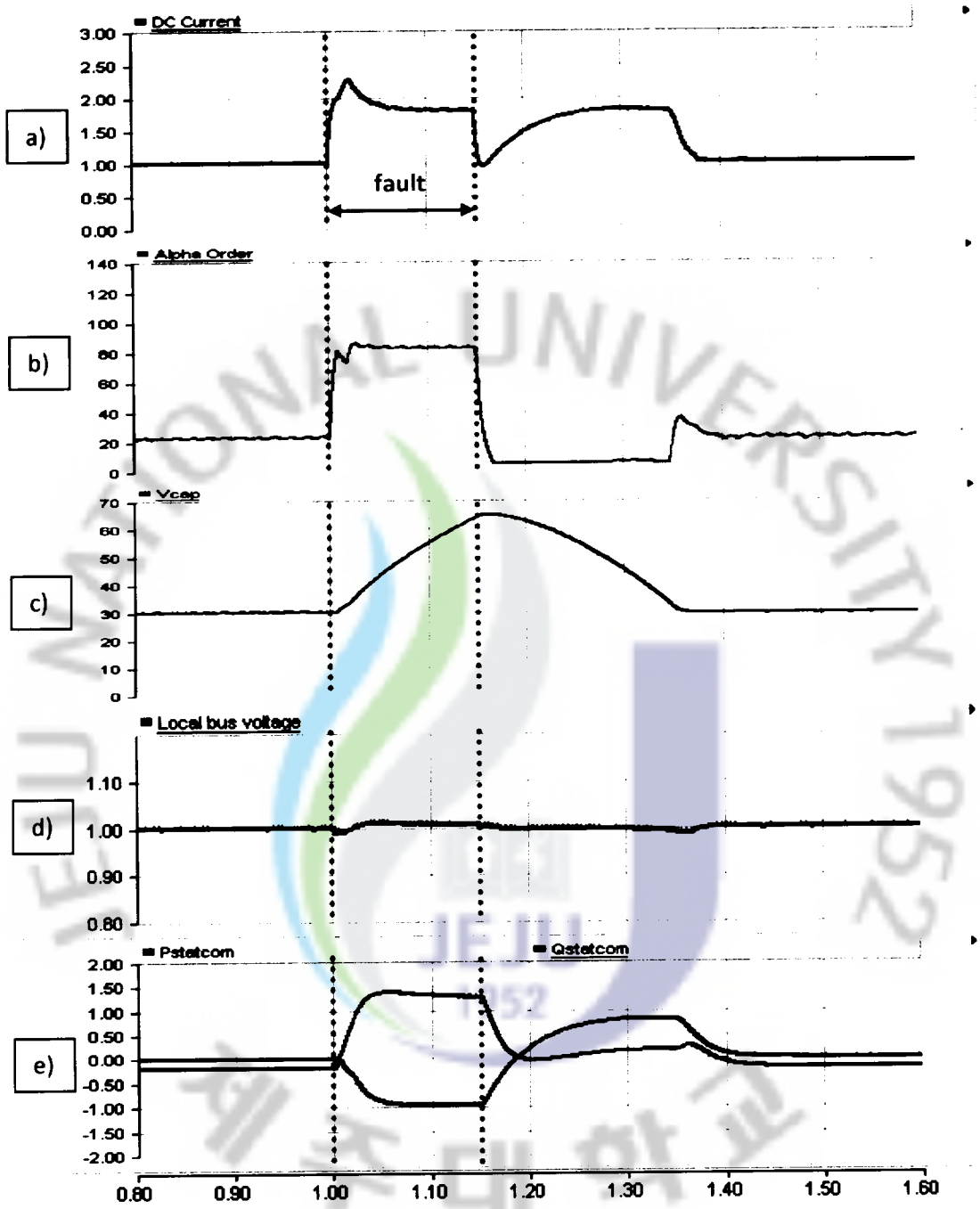

Fig. 4.2 Control system performance during a fault without the SSC.

a) HVDC DC-link current (p.u.). b) Rectifier firing angle (degree).

c) STATCOM DC-link voltage (kV). d) Local bus voltage (p.u.).

e) STATCOM active and reactive power (p.u.).

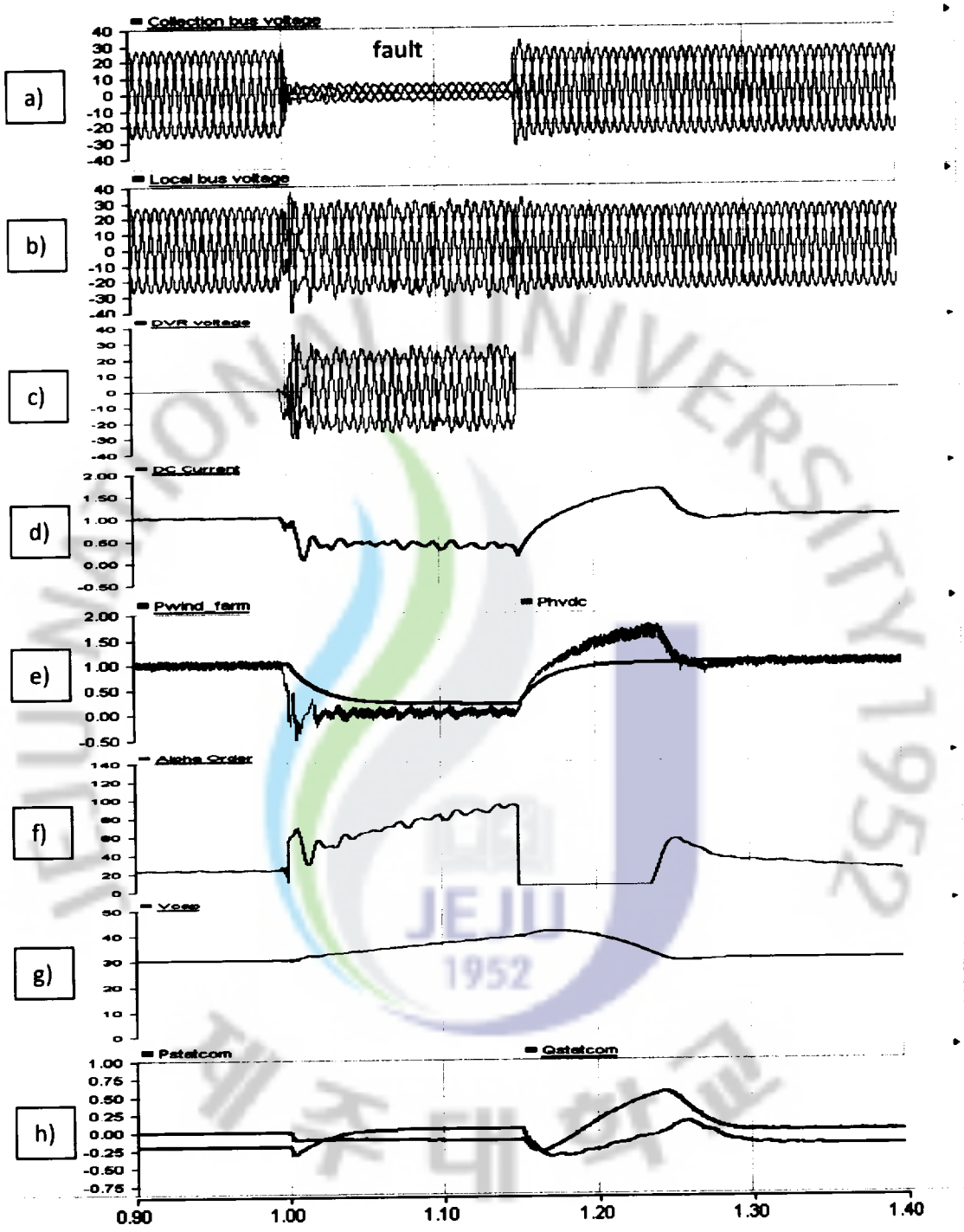

Fig. 4.3 Control system performance during a fault without the local load.

a) Collection bus voltage (kV). b) Local bus voltage (kV).

c) Controllable voltage of SSC (kV). d) HVDC DC-link current (p.u.). e) Active power generated from the wind farm and active power transferred through HVDC (p.u.).

f) Rectifier firing angle (degree). g) STATCOM DC-link voltage (kV). h) STATCOM active and reactive power (p.u.).

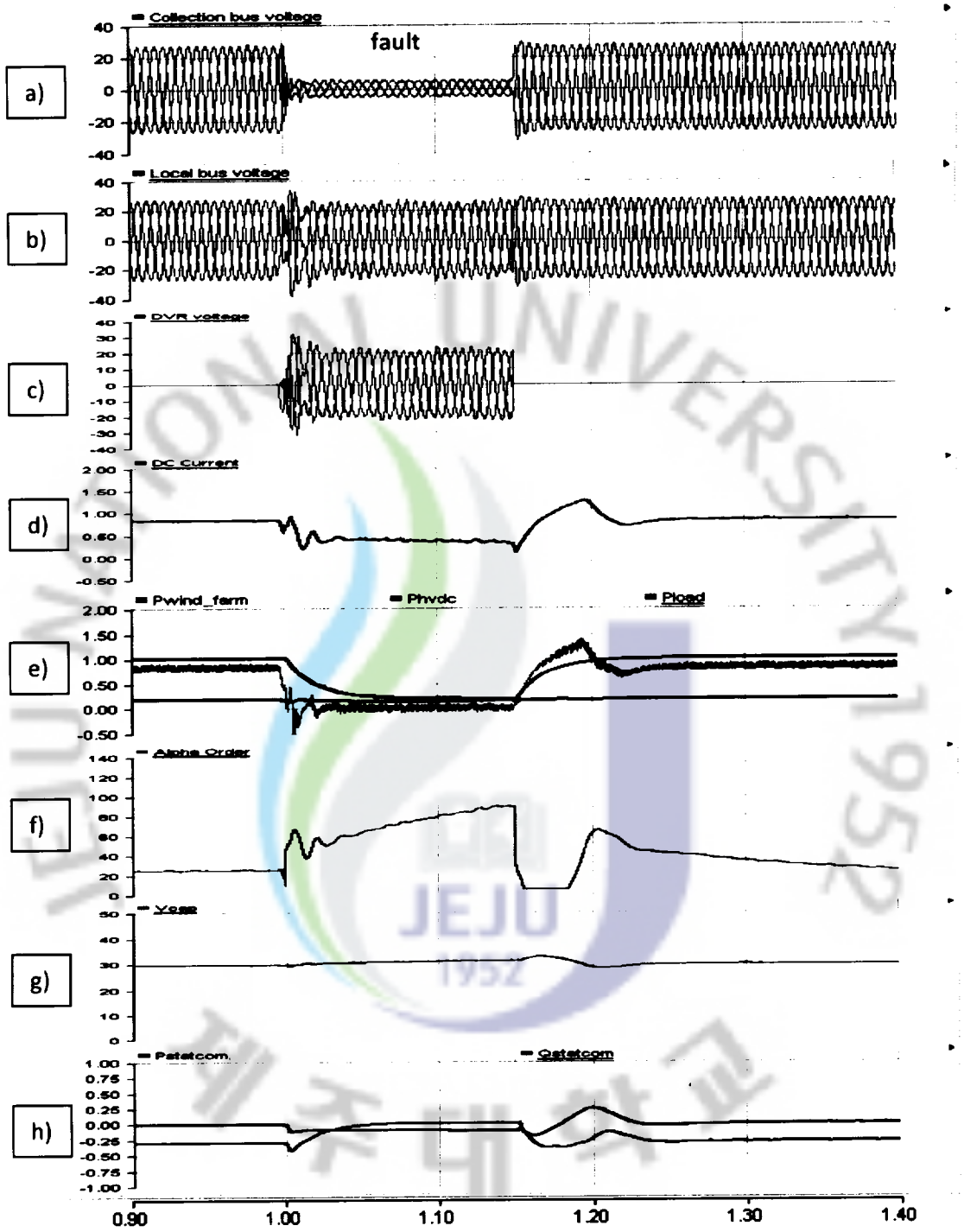

Fig. 4.4 Control system performance during a fault with the local load.

a) Collection bus voltage (kV). b) Local bus voltage (kV).

c) Controllable voltage of SSC (kV). d) HVDC DC-link current (p.u.). e) Active power generated from the wind farm and active power transferred through HVDC (p.u.).

f) Rectifier firing angle (degree). g) STATCOM DC-link voltage (kV). h) STATCOM active and reactive power (p.u.).

5. Conclusions

The thesis considered the grid voltage control system for a large offshore wind farm with a LCC HVDC connection to the main onshore network with special consideration of the serious fault. The control system provides high performance control of the offshore AC grid, and guarantees transfer of generated wind power into the main onshore grid. Especially, in the worst case of a three-phase-to-ground fault on the onshore grid, the control system proved its good performance and that it is an optimal solution. The controlled plant's detailed nonlinear mathematical model was derived and transformed into appropriate linear form for convenient control design. The equations for controller design and the control block diagram structure were derived. Simulations using PSCAD/EMTDC software illustrated system performance under normal operation and fault conditions, and verified the control design procedure. The thesis's control system can be a satisfactory solution for integrating large offshore DFIG-based wind farms into existing AC networks; especially when local load is sensitive and always require a continuous power supply with high quality demand.

The method used in this thesis is based on the idea that by lowering the wind farm network voltage a power reduction is automatically effected. Since the wind farm network voltage is highly controllable, a reduction of the wind farm voltage amplitude is possible within several milliseconds complying with the Grid Code. However, this method has also several serious drawbacks.

Firstly, the voltage reduction method works best if the wind farm consists of wind turbine generators that are variable speed machines employing a power electronic converter, such as the DFIG or various designs with a full-converter interface. The converters in these machines usually have current limits that are close to their rated current; they have hardly any over-loading capability. The concept of this strategy is that at a low network voltage the

converters of the wind turbine generators run into their current limit and the power output is changed accordingly.

Secondly, the controller design of the wind turbines needs to be adapted such that no additional voltage support is enabled, and no additional fault ride-through measures are activated. This especially holds for DFIG turbines, where a steep voltage sag might trigger the so called crow-bar protection that short-circuits the rotor windings in order to protect the converter. When the crow-bar is activated high current peaks will occur, which works adversely on the power reduction strategy.

Moreover, if the wind turbine generators are of a fixed-speed design based on directly coupled induction machines, voltage reduction may have an adverse effect. If the blade pitch controller is slow, or the machine is based on passive-stall control, it would accelerate during the low-voltage period. A high slip would occur and would load to high reactive currents, comparable to the currents that occur at starting of the machine and could be in the range of several times the rated current.

References

[1] T. Ackermann, Wind Power in Power Systems, John Wiley and Sons Ltd., England.

[2] N. Kirby, L. Xu, M. Lucket, and W. Spiemann, "HVDC Transmission for Large Offshore Wind Farms", IEE Power Engineering Journal, Vol. 9, No. 4, pp. 135-141, 2002.

[3] B. Normark and E. K. Nielsen, "Advanced Power Electronics for Cable Connection of Offshore Wind", paper presented at Copenhagen Offshore Wind 2005.

[4] Foster. S, Lie Xu, Fow. B, "Control of an LCC HVDC System for Connecting Large Offshore Wind Farms with Special Consideration of Grid Fault", in Proc. IEEE Power and Energy Society General Meeting, pp. 1-8, July 2008.

[5] Serhiy V. Bozhko, Ramón Blasco-Giménez, Risheng Li, Jon C. Clare, and Greg M. Asher, " Control of Offshore DFIG-Based Wind Farm Grid With Line-Commutated HVDC Connection", IEEE Transactions on Energy Conversion, Vol. 22, No. 1, pp. 71-78, March 2007.

[6] Risheng Li, Serhiy Bozhko and Greg Asher, "Frequency Control Design for Offshore Wind Farm Grid with LCC-HVDC Link Connection", IEEE Transactions on Power Electronics, Vol. 23, No. 3, pp. 1085-1092, May 2008.

[7] Dawei Xiang, Li Ran, Jim R. Bumby, Peter J. Tavner, and Shunchang Yang, "Coordinated Control of an HVDC Link and Doubly Fed Induction Generators in a Large Offshore Wind Farm", IEEE Transactions on Power Delivery, Vol. 21, No. 1, pp. 463-471, Jan. 2006.

[8] Ralph L. Hendriks, Ronald Volzke, and Wil L. Kling, "Fault Ride-Through Strategies for VSC-Connected Wind Parks", Proceedings of EWEC conference in Marseille, France 16-19 March 2009.

[9] Hilmy Awad, Jan Svensson, and Math Bollen, "Mitigation of Unbalanced Voltage Dips Using Static Series Compensator" IEEE Transactions on Power Electronics, Vol. 19, No.

3, pp. 837-846, May 2004.

[10] I. Erlich, W. Winter, and A. Dittrich, "Advanced Grid Requirements for the Integration of Wind Turbines into the German Transmission System", IEEE Power Engineering Society General Meeting, 2006.

[11] M. H. Bollen, "Voltage, Power and Current Ratings of Series Voltage Controllers", IEEE Power Engineering Society Winter Meeting, Vol. 4, pp. 2910-2915, 2000.

[12] M. Szechtman, T. Wess, and C. V. Thio, "First Benchmark Model for HVDC Control Studies", CIGRE Committee, Electra, Vol. 14, No. 135, pp. 56-73, 1998.